

Widespread biochemical reaction networks enable Turing patterns without imposed feedback

Received: 12 February 2024

Accepted: 11 September 2024

Published online: 27 September 2024

 Check for updatesShibashis Paul^{1,2}, Joy Adetunji¹ & Tian Hong²✉

Understanding self-organized pattern formation is fundamental to biology. In 1952, Alan Turing proposed a pattern-enabling mechanism in reaction-diffusion systems containing chemical species later conceptualized as activators and inhibitors that are involved in feedback loops. However, identifying pattern-enabling regulatory systems with the concept of feedback loops has been a long-standing challenge. To date, very few pattern-enabling circuits have been discovered experimentally. This is in stark contrast to ubiquitous periodic patterns and symmetry in biology. In this work, we systematically study Turing patterns in 23 elementary biochemical networks without assigning any activator or inhibitor. These mass action models describe post-synthesis interactions applicable to most proteins and RNAs in multicellular organisms. Strikingly, we find ten simple reaction networks capable of generating Turing patterns. While these network models are consistent with Turing's theory mathematically, there is no apparent connection between them and commonly used activator-feedback intuition. Instead, we identify a unifying network motif that enables Turing patterns via regulated degradation pathways with flexible diffusion rate constants of individual molecules. Our work reveals widespread biochemical systems for pattern formation, and it provides an alternative approach to tackle the challenge of identifying pattern-enabling biological systems.

Self-organized pattern formation is a fundamental concept in cell biology, development, and regeneration. In 1952, Alan Turing proposed a mathematical framework for pattern formation based on chemical reactions among diffusive substances¹. These reaction-diffusion systems can deviate from a spatially homogeneous steady state upon small perturbations, and transition to a stable state with a periodic pattern known as a Turing pattern (Fig. 1a). Turing patterns have been used to explain a diverse range of intriguing biological phenomena, such as hair follicle formation, digit morphogenesis, fingerprint, feather development, skin patterns, and widespread symmetries in biology (e.g. flower and leaf structures)^{2–8}. Although there are other pattern-enabling mechanisms that are also consistent with

mathematical and biological principles^{9–11}, they can often work in concert with Turing pattern to support development^{12–15}. Recent work with homogenized *X. laevis* egg extracts showed that self-organization of cytoplasm into cell-like compartments can occur in the absence of preformed cellular boundaries⁶, which further suggests the importance of continuum-like reaction-diffusion systems in embryonic development. Nonetheless, specific reaction-diffusion systems that govern most of the Turing-patterns-like structures remain poorly understood.

In 1972, Gierer and Meinhardt proposed an intuitive model for the molecular mechanisms underlying Turing patterns: a two-component reaction-diffusion system containing an 'activator' molecule with low

¹Department of Biochemistry & Cellular and Molecular Biology, The University of Tennessee, Knoxville, TN 37916, USA. ²Department of Biological Sciences, The University of Texas at Dallas, Richardson, TX 75080, USA. ✉e-mail: hong@utdallas.edu

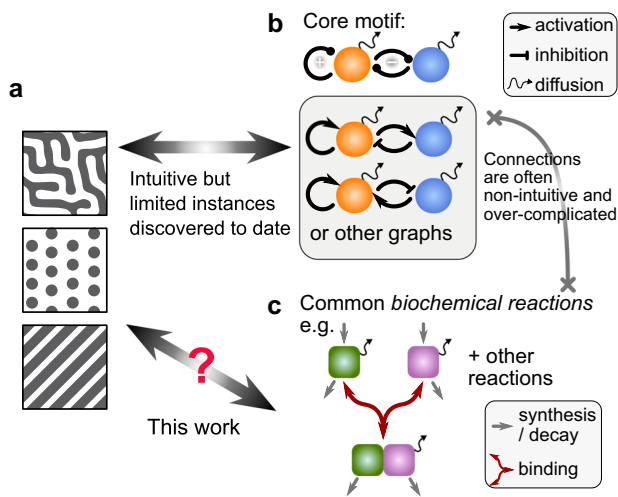


Fig. 1 | A comparison of previous approaches and this work. **a** Examples of Turing patterns. **b** Previous approaches of using signed directed graphs (gene regulatory networks) to generate intuition and to identify specific molecular systems governing Turing patterns. **c** Common biochemical reaction networks based on synthesis, degradation and binding that do not have general correspondence to signed directed graphs. The goal of this study is to identify widespread reaction networks capable of generating Turing patterns.

diffusion rate and an ‘inhibitor’ molecule with high diffusion rate (Fig. 1b box)¹⁷. This model was extended into a widely accepted “rule of thumb” for Turing pattern formation: a combination of long-range negative feedback and short-range positive feedback (defined as activator-negative-feedback here) (Fig. 1b)^{18,19}. This intuitive requirement of a two-component system is consistent with Turing’s mathematical concept, and it enabled the identification of some of the specific systems governing pattern formation. However, despite decades of efforts to connect the theory-driven intuition to biological phenomenon, very few activator-negative-feedback systems (Fig. 1b) have been identified and rigorously verified with experiments²⁰. The scarcity of these molecular systems discovered to date contrasts sharply with the widespread biological patterns potentially explainable by the concept of Turing pattern formation.

Recent theoretical studies have expanded the possibilities of molecular systems underlying Turing patterns. For example, pattern-enabling regulatory networks containing three molecules (nodes) were systematically explored^{21–23}. While these studies are useful to understand Turing patterns driven by systems beyond two-component systems, the proposed gene regulatory networks are still directly underpinned by the activator-negative-feedback intuition (Fig. 1b). Similarly, a recent study that identified minimal pattern-enabling systems with mass-action kinetics also used a two-component, activator-negative-feedback framework²⁴. At the fundamental level, these approaches rely on the abstraction of complex molecular interactions into signed directed graphs (Fig. 1b) for making connections to specific biological systems. In these graphs, one molecular regulation (edge) involves only a pair of nodes, each of which is either an activator or an inhibitor. As a result, the activator-negative-feedback concept remains to be the only intuitive model for identifying Turing systems in biology to date. In most biochemical reactions, however, it is difficult to recognize activator and inhibitor, and this has been a long-standing challenge to bridge Turing’s theory and real-world mechanisms in biochemical systems²⁵. It is therefore unclear whether there are common biochemical reactions, including those not readily described by graphs (e.g. reactions in Fig. 1c and their variants), that can produce Turing patterns.

In this work, we used the first principles of biochemistry to build models describing reaction-diffusion systems applicable to most

proteins and RNAs in multicellular organisms. These systems include production, degradation, binding, and diffusion of molecules with no activator/inhibitor identity assigned to any molecule. By analyzing these mass-action-based models, we found that a large family of reaction networks, applicable to several thousand of proteins and RNAs according to transcriptome- and proteome-wide experiments and bioinformatic analysis, can generate Turing patterns. While these networks are mathematically consistent with Turing’s theory of morphogenesis, there is no apparent connection between them and the commonly used activator-negative-feedback intuition. The simplest pattern-enabling reaction only requires the formation of a trimer molecule via sequential binding, and the altered degradation rate constants of monomers upon binding. The pattern-enabling models not only captured well-known diffusive proteins involved in morphogenesis, but also predicted roles of various other molecules and processes, such as mobile RNAs and post-transcriptional regulations, which were previously underappreciated in tissue patterning. Our work reveals unexpected, widespread molecular systems for pattern formation, and it provides a novel approach to tackle the long-standing challenge of connecting Turing’s theory to specific biological systems.

Results

A systematic search for Turing pattern enabling reaction networks without imposed feedback

To address the question of whether common biochemical reactions with no apparent feedback loop can generate Turing patterns, we first enumerated 11 basic types of biochemical “complexes” formed by noncovalent interactions between regulatory molecules such as RNAs and proteins (Fig. 2a, 11 icons with various numbers of circles). These complexes correspond to all topologically distinct configurations with up to four subunits (e.g., protein chains and RNA molecules) (denoted as A, B, C and D or the four types of circles in Fig. 2a. see Methods). We next considered elementary reaction networks that lead to the formation of the complexes via binding. Each complex in Fig. 2a can be viewed as the “final product” of each reaction network and is defined as *characteristic complex* with respect to the network. In addition to binding and unbinding, each network includes constant synthesis of the unbound molecules, degradation of each molecule in each complex, and diffusions of all chemical species (e.g., Fig. 2a callout). The inclusion of production and degradation is because the timescale of pattern formation process in biology is often comparable to or slower than typical half-lives of RNAs and proteins (see Methods). We described each reaction with mass-action kinetics. The 11 characteristic complexes (Fig. 2a) and their associated reactions (e.g. Fig. 2a callout) are fundamental processes applicable to virtually all biomolecules in cells. Of note, these networks are different from previous graph-based approaches for studying Turing systems in that the networks chosen here describe regulations at post-synthesis stages, which typically correspond to post-transcriptional and post-translational processes widespread in biology, whereas transcriptional networks (i.e. genes turning each other ‘on/off’) and their associated graphs were often used in previous studies^{21–23}. Our modeling framework also differ from previous mass-action based models^{24,26}, i.e., we explicitly describe complex formation as an elementary and ubiquitous biochemical reaction, and we do not attempt to produce Turing patterns from minimal systems that can be interpreted directly with the activator-negative-feedback concept. Our goal is to test whether each reaction network leading to the formation of characteristic complexes can produce Turing patterns with biologically plausible parameter values.

While the 11 complexes allow us to examine biochemical reactions with various complexities, each complex may be formed by multiple sets of binding events (e.g. $AA + B \rightarrow AAB$ or $AB + A \rightarrow AAB$). As a result, 23 distinct networks (i.e. reaction paths) leading to the formation of the 11 complexes were included in our analysis (Fig. 2b. Production and

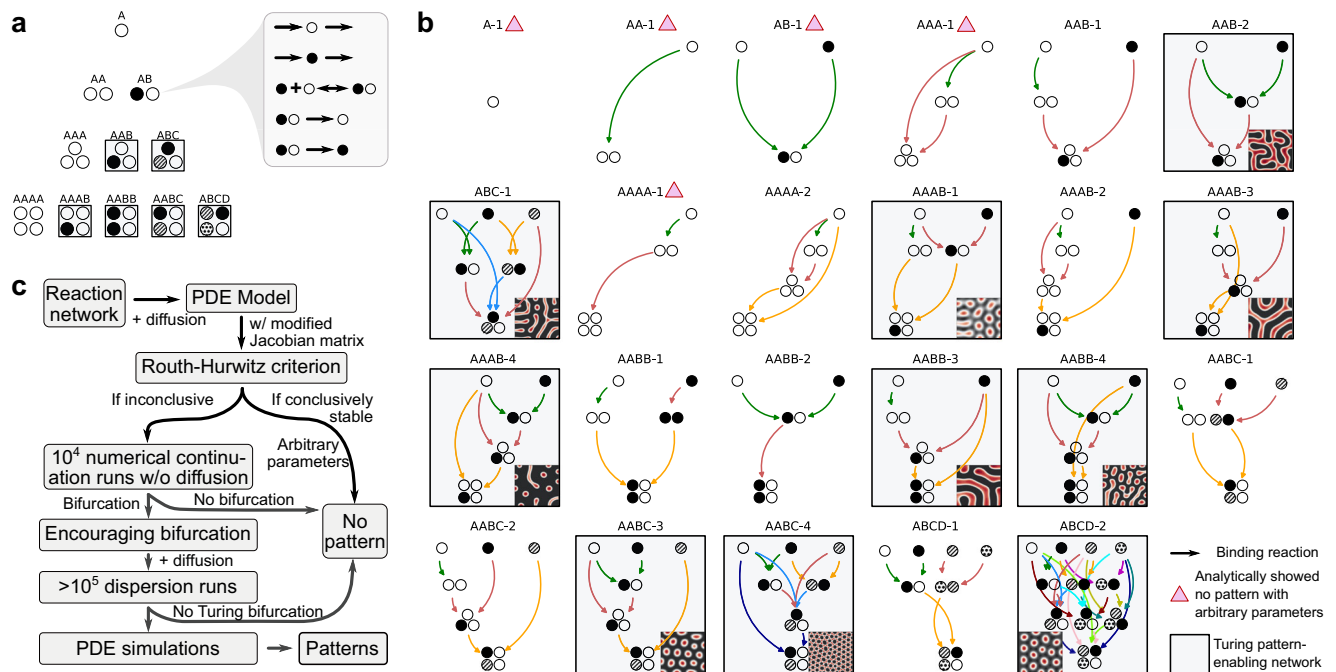


Fig. 2 | A screen for pattern-enabling reaction networks. **a** 10 complexes with various configurations containing 1–4 subunits (circles). Callout shows an example of reaction networks associated with a characteristic complex. Square boxes show pattern-enabling complexes (see B and C for procedures leading to these conclusions). **b** Illustration of binding reactions in networks (paths, models) leading to complexes shown in A. Each color of arrows in a network corresponds to one binding reaction. Synthesis, degradation, and diffusion of each subunit are not shown but are included in models. Triangles indicate networks analytically shown to be incapable of producing Turing patterns. Boxes show pattern-enabling

networks (see C for procedures leading to these conclusions). Inset boxes display examples of stationary patterns illustrating concentrations of free B at time 500 and a box length of 100, simulated with a temporal step size of 10^{-4} and a spatial grid size of 1.0. The physical interpretations of time and space are described in Supplementary Information. Color gradients are normalized across the 10 models, but the minimum range (max-min) is 0.26 units of concentration. **c** A flowchart for screening reaction networks capable of producing Turing patterns (see Methods for details). Source data are provided as a Source Data file.

degradation not shown). We built a mathematical model for each network with mass-action kinetics using ordinary differential equations (ODEs). We further extended these models to include Fickian diffusion of all molecules, which gave rise to the partial differential equations (PDEs) (see Methods and Supplementary Information). The models contain 1–11 variables representing concentrations of molecular species.

Using analytical approaches such as the Routh-Hurwitz Criterion^{27,28}, we found that five networks cannot generate any Turing pattern with arbitrary positive rate constants (see Methods and Supplementary Information) (Fig. 2b, pink triangles; Supplementary Figs. S1–S3). For each of the remaining 18 reaction paths (models), we used a computational pipeline (Fig. 3c; Supplementary Fig. S4) to search for possible parameter sets that can generate Turing patterns. It has been shown that Turing patterns (stationary periodicity in space) often appear below the instability threshold of Hopf bifurcations at the temporally stable regions, whereas limit cycle oscillations (periodicity in time) are observed above the instability threshold of Hopf bifurcation^{29–31}. Albeit Turing patterns can be observed even in the absence of Hopf bifurcation, to enhance the efficiency of the computational pipeline we first considered only the reaction, but not the diffusion, terms in our models, and asked whether the ODE system for each reaction network (path) can generate Hopf bifurcations. We selected 10,000 parameter sets for each ODE system and performed numerical continuation for each set to find Hopf bifurcations. These parameter sets were randomly chosen from biologically plausible ranges covering two orders of magnitude (see Methods; Supplementary Table S1). The Hopf bifurcations served as the “encouraging” bifurcation that allowed us to search for Turing bifurcation efficiently. For reaction paths that produced Hopf bifurcations, we added the

diffusion terms back into the models, which yielded systems of PDEs. We randomly sampled diffusion coefficients, and identified Turing pattern-enabling parameter sets by analyzing dispersion relations and simulating the PDEs numerically (see Methods) (Fig. 2c)^{21,22,32–34}.

Among the 18 reaction networks with inconclusive algebraic analysis, we found that 10 of them, corresponding to 6 characteristic complexes, produced Hopf bifurcations with biologically plausible parameters (Fig. 2a, b boxes). While none of these paths contains any imposed negative feedback loop often considered a requirement for oscillation (Hopf bifurcation), our results are consistent with recent studies that showed the abilities for post-transcriptional and post-translational reaction networks to generate oscillation without imposed feedback^{35–37}. All 10 PDE models derived from the Hopf bifurcation-enabling reaction networks also produced Turing patterns with some combinations of reaction parameters and diffusion coefficients (Fig. 2b, boxes; Fig. 3a; Supplementary Data 1 and Supplementary Data 2). Overall, for the 10 Turing pattern-enabling models, 2% of the randomly generated ODE parameter sets gave rise to Hopf bifurcations, and 0.13% of parameter sets for the full reaction-diffusion systems produced Turing patterns (Fig. 3a; Supplementary Fig. S6). The latter fraction is comparable to a previous study for quantifying the robustness of activator-inhibitor Turing systems²¹. Nearly all parameter sets with Hopf bifurcation produced Turing patterns with some combinations of diffusion coefficients (Supplementary Fig. S7), and unsurprisingly, there was a positive correlation between percentages of Hopf bifurcations and Turing patterns across the models (Fig. 3a). Although parameter sets that did not produce Hopf bifurcations in ODE models can also generate Turing patterns in PDE models, the percentage of pattern-enabling sets in this group was very low (<3%). We therefore did not include dispersion analysis for the

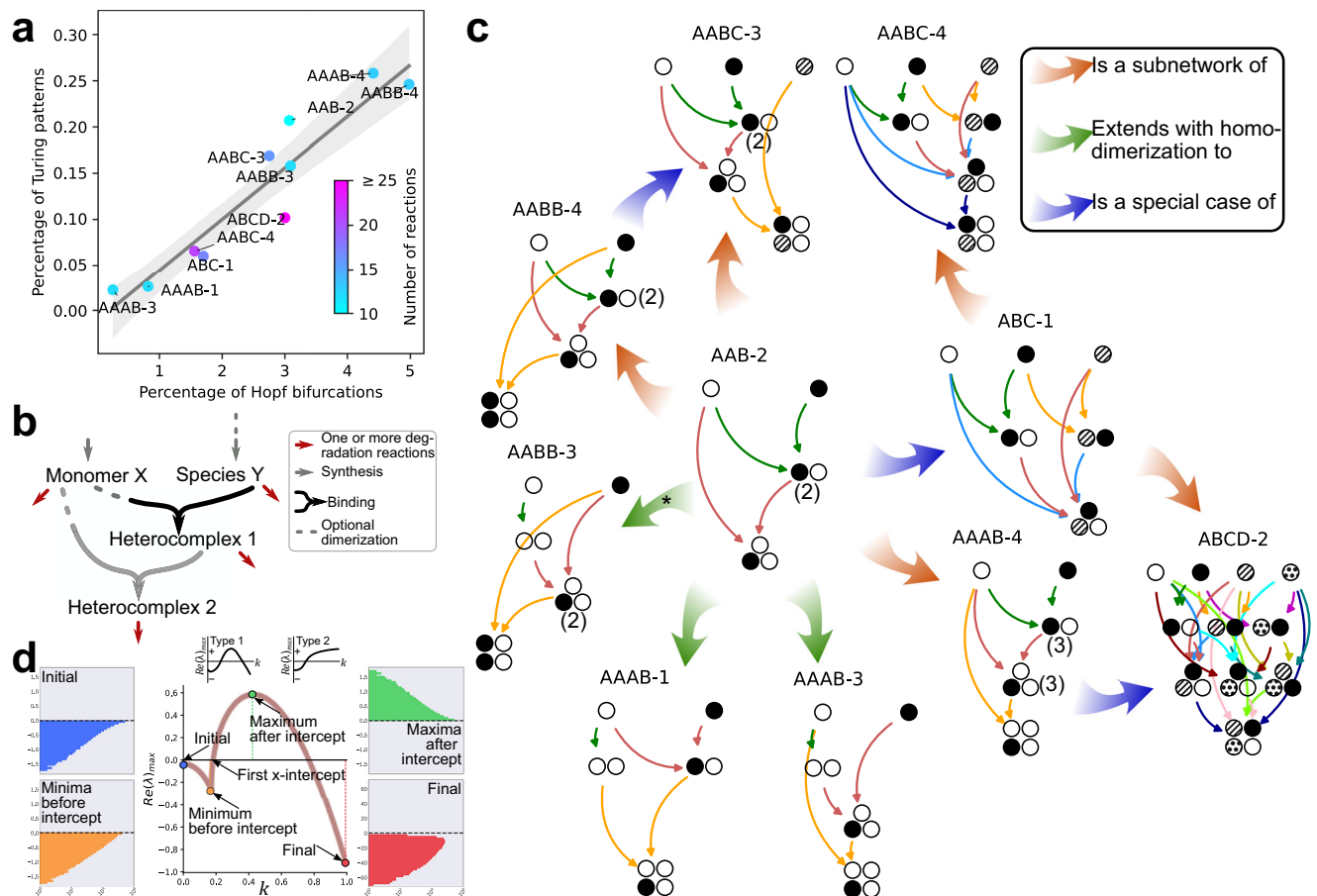


Fig. 3 | Topological requirements for pattern-enabling reaction networks. **a** Percentages of parameter sets that produced Hopf bifurcations and those that produced Turing patterns for 10 pattern-enabling networks. Light gray area shows 95% confidence interval of the linear regression line (dark gray). **b** A unified network motif of 10 pattern-enabling reaction networks. **c** Topological relationships of all pattern-enabling reaction networks. Numbers in parentheses show multiplicities of

molecules with the same configurations. **d** Distributions of terminal points of the complete set of Turing pattern-enabling dispersion curves (505,125 pattern-enabling sets) for detecting possible existence of two types of dispersion curves (presence of the red points' positional distribution in the positive range would have implied the fractional occurrence of the Type 2 dispersion curves). Source data are provided as a Source Data file.

bifurcation-free ODE set in our main computational pipeline for efficiency considerations (Fig. 2c). Taken together, our results show that a wide range of basic biochemical reactions can produce Turing patterns without any imposed feedback loop (see Discussion for a comparison between explicit and implicit feedback).

Network topology required for Turing pattern-enabling reactions

Our high-throughput network and parameter scanning allows us to examine the requirements for the reaction networks to achieve Turing patterns. In this section, we describe requirements in terms of network structures. In the next section, we will discuss the requirements of kinetic rate constants.

Each of the 10 pattern-enabling reaction networks contain at least two different molecules (Fig. 2b, black and white circles). Note that in the model, different molecules specifically refer to molecules with different parameters such as degradation rate constants (The parameter values differ by up to 100 folds, e.g. Supplementary Fig. S8. See next section for detailed analysis). Furthermore, the characteristic complex of a pattern-enabling reaction network is either heterotrimers or heterotetramers (Fig. 2b). Most interestingly, we found that a simple network motif is present in each pattern-enabling network and absent in each network that failed to produce a pattern (Fig. 3b). This motif contains a monomer that is sequentially involved in the formation of two heterocomplexes in a 'feed-forward' manner (Fig. 3b, Monomer X).

Reaction network AAB-2 is the simplest reaction network that contains this motif, while other pattern-enabling networks are connected to this motif via three distinct ways: 1) a smaller pattern-enabling network (AAB-2 or its derivative) is a subnetwork of a larger pattern-enabling network (Fig. 3c, orange arrows); 2) a pattern enabling network is expanded by homodimerization of a molecular species to generate another pattern-enabling network (Fig. 3c, green arrows); and 3) a pattern enabling network is a special case of a general pattern-enabling network that has more types of subunits (Fig. 3c, blue arrows).

It should be noted that the networks in our study are hypergraphs (each edge that represents binding involves 3 nodes) rather than regular graphs commonly used for defining feed-forward loops. These two types of graphs have very different mathematical properties. We therefore do not claim that we found pattern-enabling feed-forward loops. Nonetheless, the simple motif shown in Fig. 3b (see later sections for its prevalence in biology) is sufficient for distinguishing the pattern-enabling networks from all other ones used in our search, and these results showed that network topology is important for Turing pattern formation even in the absence of imposed feedback and activator-inhibitor identities.

It was shown that there are two types of instability for Turing patterns (Type 1 and Type 2) that can be revealed by dispersion analysis. The systems showing Type 1 variant of Turing instability remain stable at small length scale perturbations and characterized by non-zero diffusion of all the molecules comprising the system³⁸, whereas

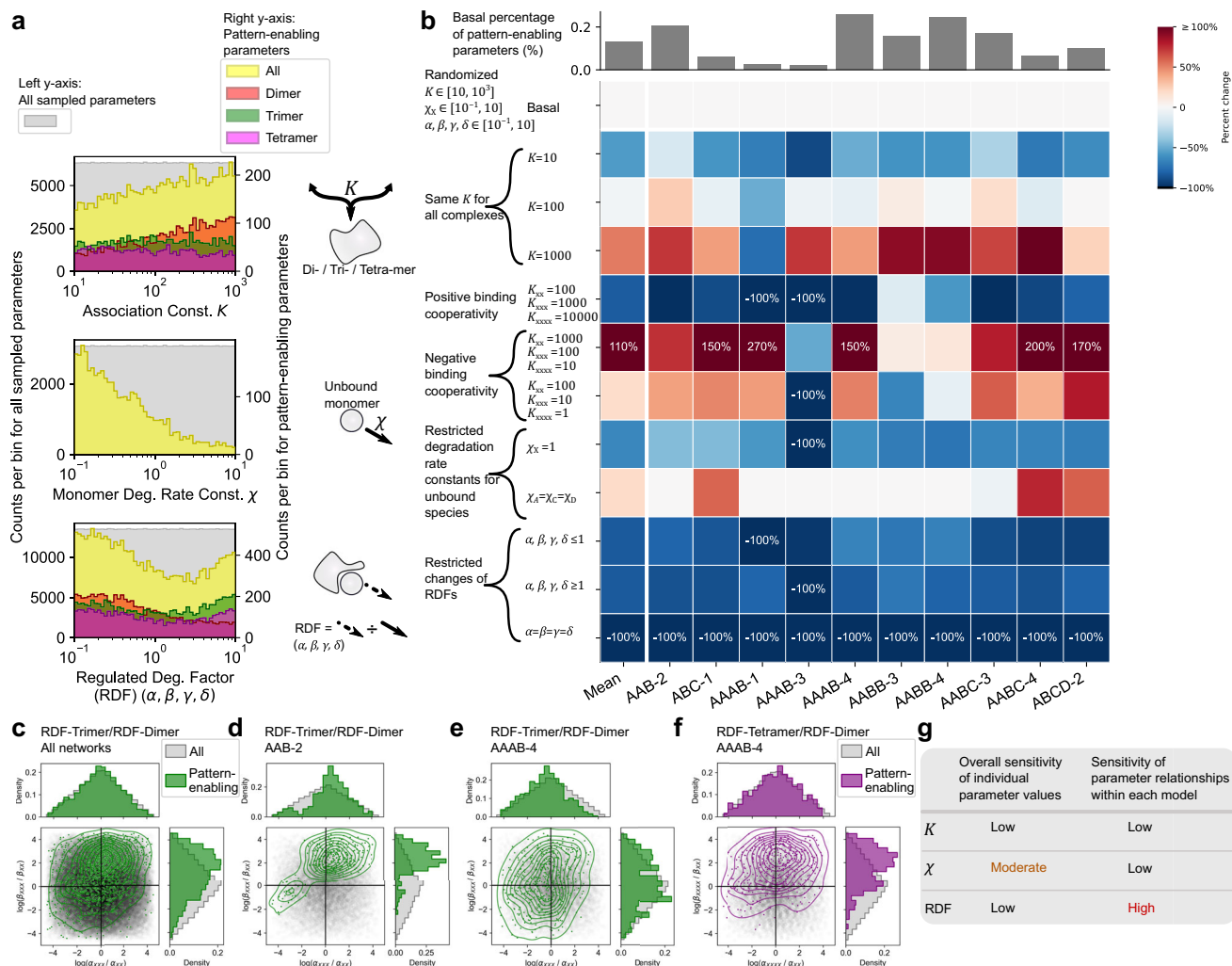


Fig. 4 | Distributions of reaction parameters enabling patterns. **a** Distributions of three types of parameters in all 10 pattern-enabling models. All sampled parameters (gray) and those enabling patterns (colored) are in scales shown in the left and right axes, respectively. The right diagrams show the meanings of the parameters. **b** Top chart shows percentages of pattern-enabling parameter sets with randomly chosen values from ranges shown on the left (Basal ranges). Heatmap

shows the changes of the percentages when the ranges were perturbed. For each perturbation, the computational pipeline shown in Fig. 2c was rerun to obtain the percentages. **c–f** distributions of RDFs in two types of complexes in all (c) and two selected models (d–f). **g** Summary of sensitivities of three types of reaction parameters. Source data are provided as a Source Data file.

Type 2 instability is associated to the systems comprising one or more non-diffusive molecules^{21,22,39}. Because all pattern-enabling networks have the same origin in terms of their topologies (Fig. 3b, c), we hypothesized that they are of the same Turing pattern type. We therefore analyzed the dispersion curves of all pattern-enabling parameter sets for all networks. We found that all of them produced Turing in each complex (α, β, γ , and δ with subscripts representing complexes) with respect to the corresponding monomer. We found that while it is more likely for models with greater binding affinities (K), particularly with dimer formation, to generate patterns, patterns were observed in a wide range of K (Fig. 4a, top). In contrast, lower monomer degradation rates with respect to B markedly enhanced the likelihood of pattern formation (Fig. 4a, middle). Nonetheless, patterns were observed across two orders of magnitudes of these rate constants. In addition, we found that different molecules can have significantly different monomer degradation rate constants in those pattern-enabling sets even if the two molecules (e.g. A and C in the ABC-1 model) have similar reactions in the network (Supplementary Fig. S8). Interestingly, we found more pattern-enabling parameter sets with lower degradation rates in complexes (i.e. RDFs) in dimers, whereas the ability for pattern formation did not depend strongly on other individual RDFs (Fig. 4a, bottom).

Kinetic rate constant requirement for Turing pattern-enabling reactions

With the 10 pattern-enabling reaction networks, we asked whether Turing patterns were observed in a specific range of each parameter. Because the 10 networks have different numbers of parameters, we analyzed three major groups of parameters instead of individual parameters: 1) scaled association constants (denoted by K with

subscripts representing complexes) reflecting the binding affinities; 2) scaled degradation rate constants for monomer A, C and D (denoted as χ_A, χ_C and χ_D , which were scaled with respect to monomer B's degradation rate constant); and 3) relative degradation rate constants (also defined as regulated degradation factors, i.e. RDFs) of each molecules with respect to the corresponding monomer. We found that while it is more likely for models with greater binding affinities (K), particularly with dimer formation, to generate patterns, patterns were observed in a wide range of K (Fig. 4a, top). In contrast, lower monomer degradation rates with respect to B markedly enhanced the likelihood of pattern formation (Fig. 4a, middle). Nonetheless, patterns were observed across two orders of magnitudes of these rate constants. In addition, we found that different molecules can have significantly different monomer degradation rate constants in those pattern-enabling sets even if the two molecules (e.g. A and C in the ABC-1 model) have similar reactions in the network (Supplementary Fig. S8). Interestingly, we found more pattern-enabling parameter sets with lower degradation rates in complexes (i.e. RDFs) in dimers, whereas the ability for pattern formation did not depend strongly on other individual RDFs (Fig. 4a, bottom).

To interrogate the dependence of pattern formation on the cooperativities of parameters, we perturbed the parameter ranges with various imposed restrictions, and performed the computational searches for Turing patterns with the perturbed ranges (Fig. 4b). We found that binding cooperativity is not required for pattern formation, i.e., all complexes in a model can be formed with the same binding affinity without losing the capacity of pattern formation. There was a simple positive correlation between binding affinity and percentages of pattern-enabling parameter sets in all 10 networks (Fig. 4b). Interestingly, highly positive binding cooperativity (i.e. higher binding affinities in higher order complexes) dramatically decreased the percentages of pattern-enabling parameter sets for most networks (Fig. 4b). In contrast, negative binding affinities generally increased the percentages of pattern-enabling parameter sets even if the overall binding affinities were lower than the unperturbed ones (Fig. 4b). We observed that these perturbations had different extents of impact on the 10 pattern-enabling networks. For example, the AAB-3 network had an exceptionally low sensitivity to the perturbation to positive cooperativity. Similar to most other networks, the AAAB-1 network had significantly higher percentages of pattern-enabling parameter sets upon switching to negative binding cooperativity, whereas for the AAAB-3 network, the pattern-enabling ability was reduced with the same perturbation (Fig. 4b).

Although differences among monomer degradation rate constants were not strictly required for pattern formation, equalizing all four monomers' degradation rate constants resulted in significantly lower fractions of pattern-enabling parameter sets, compared to both unperturbed conditions, as well as a perturbed condition allowing a difference between monomer B's degradation rate constants and that of other monomers (Fig. 4b). Finally, although mechanisms for complex formation can either protect all molecules from degradation or enhance their degradation for most networks (Fig. 4b), equalizing the RDFs for all molecules (i.e. all subunits degrade with the same rate constant in all complexes) completely abolished the ability of pattern formation for all networks (Fig. 4b).

The stark contrast between the perturbation by equalizing RDFs and their broad distributions among pattern-enabling parameter sets (Fig. 4a, b, bottom) suggested that pattern formation could be sensitive to the ratios, rather than individual values, of RDFs within each model. We therefore examined the distributions of trimer-to-dimer ratios of RDFs for A and B (α_{xxx}/α_{xx} and β_{xxx}/β_{xx}) under the unperturbed condition, and we found that the pattern-enabling parameter sets tend to have higher trimer-to-dimer RDF ratio for B (Fig. 4c) when parameter sets of all networks were combined. When we compared two networks containing only A and B molecules, AAB-2 and AAAB-4, we found that the pattern formation is generally correlated with higher trimer-to-dimer RDF ratios for AAB-2 but not AAAB-4 (Fig. 4d, e). However, the pattern-enabling parameter sets for the AAAB-4 network had high tetramer-to-dimer RDF ratios for B compared to the background (Fig. 4f). This shows that even though AAB-2 is a subnetwork of AAAB-4, AAB-2's requirements of RDFs for pattern formation may be replaced by those of RDFs in higher order complexes. In summary, among all three types of rate constants, pattern formation was most sensitive to ratios of RDFs, and it was significantly sensitive to the individual degradation rate constants of monomers. While network topology of binding reactions is important for pattern formation (Fig. 2b), fraction of pattern-enabling parameter sets is not very sensitive to variations of binding affinities (Fig. 4g).

We next asked whether Turing pattern formation requires differences among diffusion coefficients (D) of molecular species in a model. For the AAB-2 model, pattern-enabling parameter sets had wide distributions of diffusion coefficients of A and B monomers. There was only moderate skewness of the distributions of D_A and D_B (Fig. 5a, top callout), suggesting there was not a strong preference for slow- or fast-diffusing monomers. In contrast, the distributions of D_{AB} and D_{AAB}

were highly skewed. Patterns seem to be enabled by high D_{AB} (highly negative skewness) and low D_{AAB} (highly positive skewness) (Fig. 5a, top callout), reflecting a physically plausible scenario of critical slowdown of diffusion upon trimer formation. The preference for slow diffusion of the largest complex, and fast diffusion of the second largest complex was also observed with five other pattern-enabling networks as a general trend (Fig. 5a, top cluster in heatmap). In addition, ordered diffusion coefficients from large, slow complexes to small, fast complexes/monomers were observed in nine out of the ten pattern-enabling networks (Supplementary Fig. S9). Nonetheless, two models (AAB-3 and -4) had the opposite trend: pattern-enabling parameter sets generally had higher diffusion coefficients of the largest complex compared to those of the second largest complex (Fig. 5a, bottom callout and heatmap). In all pattern-enabling models, the monomers had weak skewness of diffusion coefficients' distributions (Fig. 5a, heatmap), suggesting that these parameters are flexible for generating Turing patterns.

To test the causal relationship between specific diffusion coefficients and pattern formation, we selected two representative pattern-enabling parameter sets for the AAB-2 model which has four molecular species. In Set I (Fig. 5b, left), the two monomers and the dimer AB have the same diffusion coefficient, and the trimer AAB has a lower diffusion coefficient. In Set II (Fig. 5c, left), Subunit B serves as a diffusion facilitator and the diffusion coefficients of the four molecular species were ordered accordingly. In both cases, when we perturbed the parameter set by equalizing the diffusion coefficients of AAB and AB, we found that the patterns were lost (Fig. 5b, c). We found that although differential diffusivity is required to achieve Turing patterns in our models, the differences among diffusion coefficients were moderate in most pattern-enabling parameter sets (Supplementary Fig. S10, Fig. 5b). In addition, our models do not assume any immobile molecules. Therefore, the requirements on differential diffusion rates in our models are less stringent than those in most conventional models of Turing patterns.

Omics-level prediction of potential biochemical complexes enabling Turing patterns

What are possible biomolecules involved in the 6 pattern-enabling complexes (Fig. 2a boxes)? To address this question, we inferred human protein complexes and mRNA-microRNA complexes as examples of high-order complexes with configurations of subunits specified in Fig. 2a. For protein complexes predicted at the proteomic level, we used data integrated from 15,000 mass spectrometry experiments and other experimental data⁴⁰. For mRNA-microRNA complexes predicted at the transcriptomic level, we used sequence-based target prediction of microRNAs⁴¹ (see Methods). We found that almost 9000 human proteins are involved in complexes that match configurations predicted to enable Turing patterns (Fig. 6a. Blue filled bars and black boxes). Similarly, nearly half of human genes' mRNA products can be potentially involved in high-order mRNA-microRNA complexes that were predicted to be pattern-enabling (Fig. 6a. Filled red bars). In particular, the pattern-enabling configuration ABC and its associated reaction network ABC-1 has most instances for both proteins and mRNAs (Fig. 6a). The predicted complexes not only include some well-known diffusive molecules crucial for development and regeneration (Fig. 6b)⁴²⁻⁴⁹, but also contain a wide range of proteins and RNAs that can enable new hypotheses of mechanisms underlying Turing pattern formation (Supplementary Data 3). Due to the lack of measured rate constants in these predicted systems, we were not able to further constrain the list of gene products that enable Turing patterns with experimental data. This qualitative inference of complexes is therefore not sufficient to identify pattern-enabling molecules definitively, and the pool of complex-associated gene products should be viewed as a preliminary set for subsequent screening in future studies. It should be noted, however, that this limitation also applies to the classical

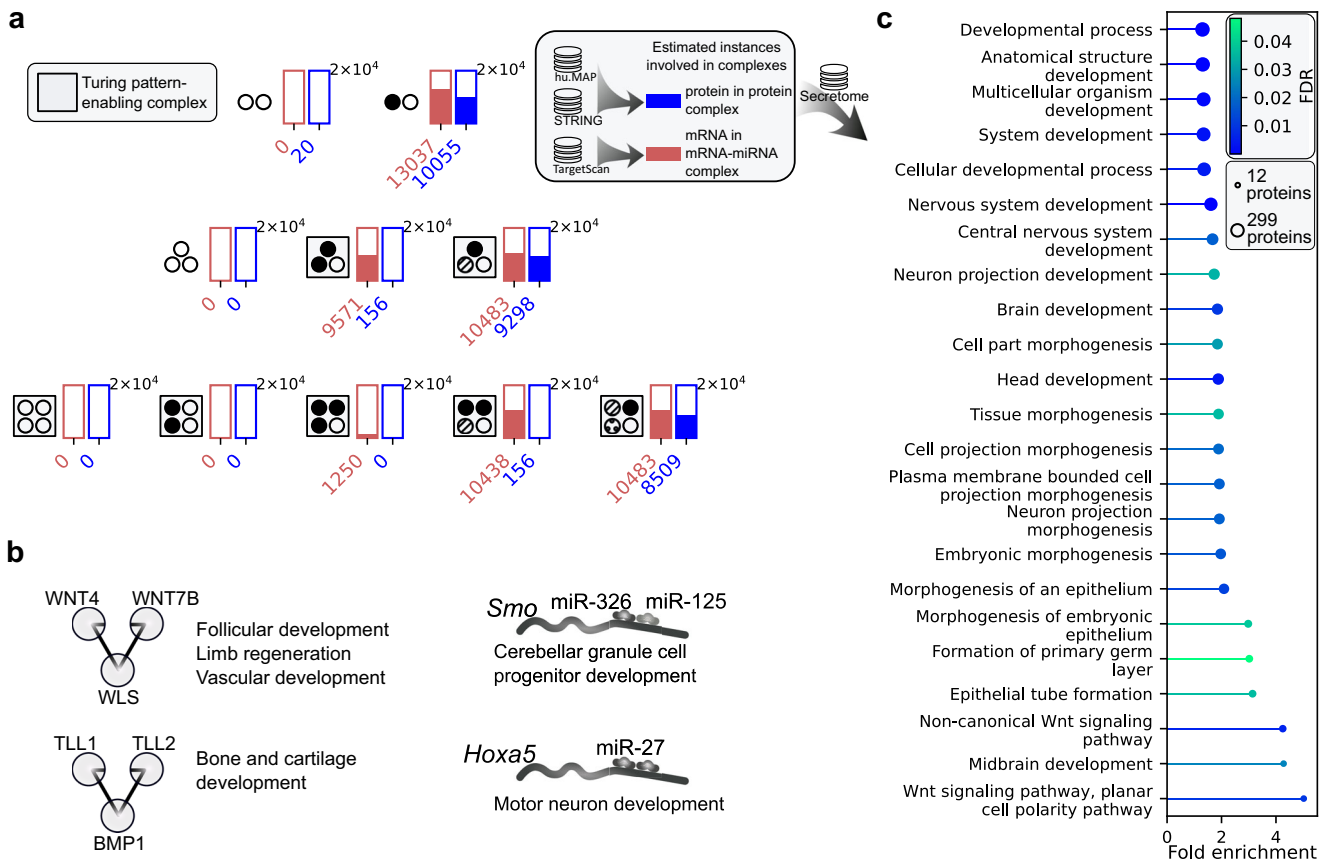


Fig. 6 | Omics-level estimation of instances of pattern-enabling complexes.

a Numbers of genes whose products are involved in protein (blue) and mRNA-microRNA (red) complexes with indicated configurations inferred from experimental data of protein interaction and sequence complementary respectively. Each bar has a maximum of 20,000, and the filled portion indicates the estimates for the configuration shown on the left. **b** Examples of protein and mRNA-microRNA

complexes that potentially enable patterns. Connecting lines in the protein complex icon indicated experimentally supported pairwise physical interaction. Known biological functions of the proteins and mRNAs are annotated. **c** Functional enrichment of secreted and membrane proteins involved in high-order configurations that potentially enable patterns (boxes in **a**). Source data are provided as a Source Data file.

activator-inhibitor paradigm for identifying systems for Turing patterns. Our findings on the broad range of proteins and RNAs whose network topologies permit Turing patterns suggest the need of measurements for key parameters, such as degradation rate constants and diffusion coefficients as shown in the previous section, for predicting Turing pattern-enabling systems more accurately.

Despite the limitation, we asked whether our prediction provides a meaningful list of proteins and RNAs that are involved in biological processes related to pattern formation. We performed functional enrichment analysis for membrane and secreted proteins which are more likely to be transported between cells⁵⁰. We found that with a background of these proteins from secretome and membrane proteome⁵¹, those involved in high-order, pattern-enabling complexes are enriched with functional terms for a wide range of developmental processes (Fig. 6c. See Methods). The mRNAs involved in high-order mRNA-microRNA complexes are also involved in many pattern-formation processes, although the folds of enrichment are moderate due to the large number of mRNAs in the gene set (Supplementary Data 4). These results suggest that pattern formation in development may be a function of proteins in high-order complexes even in the absence of explicit feedback loops of gene regulation. Nonetheless, it should be noted that there are many biological scenarios underpinned by functionally important Turing patterns besides tissue level patterning in development. The length scales of our mathematical models cover both intracellular and tissue-level patterns, so the potential biological functions arising from the complex-driven Turing patterns can be very broad (see Supplementary Information and Discussion).

Discussion

Since Gierer and Meinhardt's interpretation of self-organized pattern formation mechanism proposed by Turing¹⁷, biologists have been using the activator-feedback paradigm (Fig. 1b) to search for molecular networks supporting patterns. This intuitive connection between biological networks and Turing's mathematical concept is based on sign patterns of the Jacobian matrix at steady states of ODEs. The sign patterns are signed directed graphs that can be conveniently interpreted as gene regulatory networks (Fig. 1b and Supplementary Fig. S11). This approach is therefore widely used due to its convenience in both biology and mathematics^{21–23,52}, and the concept of pattern-enabling feedback was also extended to the mechanochemical level¹⁴. In contrast to previous studies, we show that very common biochemical reaction networks without apparent feedback structures (including autocatalysis) can generate Turing patterns. While the sign patterns of the Jacobian matrices for the underlying pattern-enabling models still contains the activator-feedback motifs (Supplementary Fig. S11), such motifs also exist in reaction networks that failed to produce patterns (e.g. AB-1, AAA-1, and AAB-1. Supplementary Figs. S11, S12). Furthermore, simple structures of biochemical reactions can give rise to overly complicated signed directed graphs that are difficult to interpret from the viewpoint of gene interactions (Supplementary Fig. S11). Our study therefore suggests a new approach for connecting Turing's theory to real-world instances of pattern-enabling biological systems. This approach is based on a simple set of signature molecular interactions (Fig. 3b) that do not depend on activations or inhibitions of molecular productions that are often used to derive pattern-enabling networks in biology.

In addition to the requirements of the simple network structure (Fig. 3b), our analysis showed that the choice of parameter values, particularly ratios between the degradation rate constants of protein/RNA subunits in various complexes, can be crucial for pattern formation. While these requirements are difficult to validate with experimental data in a high-throughput manner, altered degradation rates upon molecular binding as well as functional cooperativity upon high-order complex formation are common in biology^{53–55}. In addition to the direct interpretation of molecular degradation, the first-order decay rates of the molecules in our models can be generalized to rates of removal from a specific location (e.g. removal of molecules from plasma membrane via endocytosis⁵⁶) where patterns can arise. Nonetheless, future experiments are needed to test the models' predictions of the parametric requirements for pattern formation.

Previous studies have provided strategies to select models and/or parameters to achieve specific patterns driven by reaction-diffusion systems^{26,57}. In our work, multiple types of Turing patterns such as spots and labyrinths were observed (Fig. 2, Supplementary Fig. S4, Supplementary Data 1). While our work did not distinguish network structures or parameter values in terms of their ability to produce specific types of patterns, the expansion of reaction networks underpinning various patterns may facilitate future investigations on model selections, especially when molecular constraints are available in specific systems. Particularly, our results can help to generate new hypotheses focused on degradation/removal-based reactions rather than requiring auto-activation or other types of feedback commonly assumed for Turing pattern-enabling systems. Nonetheless, future work will be needed to compare the pattern-enabling reaction networks described in this study and previously published networks with specific constraints on details of observed patterns or molecular pathways.

Our models for pattern formation focused on systems with diffusive models only. Pattern formation at the tissue level may utilize preformed structures with molecules not diffusive across the system (e.g. gene regulation purely driven by intracellular mechanisms)^{38,58–60}. Future work is needed to investigate the relationship between the mechanism proposed in this study and hybrid systems with both diffusive and immobile molecules. Nonetheless, because our models do not require gene regulations at the production level, the spatial scales of pattern formation arising from the proposed mechanism can be at both the intracellular and the multicellular levels. Intracellular diffusion of molecules are ubiquitous and its effects on subcellular pattern formation has been studied recently⁶¹. Furthermore, our work suggests a plausible connection between Turing pattern formation and widely subcellular phase separation that may also produce periodic patterns. Tissue-level movements of proteins and RNAs are also common via mechanisms such as secretion, symplastic pathways, and extracellular vesicles^{55,62,63}, which suggests that the continuum assumption of multicellular space in our models can be realistic in some systems. Notably, the ranges of rate constants used in our models are consistent with the biologically relevant spatial scales of cells and tissues (see Supplementary Information). Overall, our study provides a new approach to connect mechanisms of Turing pattern formation to widespread biochemical reactions with no apparent structure of feedback loops. We expect that our method and predictions will facilitate discoveries of more pattern-enabling systems containing proteins and RNAs at multiple scales.

Methods

ODE model construction

We have adopted a systematic method to construct models for complex formation using mass action kinetics. In the process of model construction, we have started our scanning from the simplest possible model in the context of biochemical complex formation, i.e., complexes with only one species, and thereafter chronologically scanned

all the possible pathways leading to homomeric and heteromeric complexes constituting a maximum of four species. The entire process of scanning biochemical networks yields a sum of 23 network pathways, resulting in 11 unique complexes. The ordinary differential equations depicting the temporal dynamics of the complex formation were made dimensionless by scaling variables and parameters using degradation and synthesis rate constants of two distinct monomers (A and B, as per our formulation, were used to represent these distinct monomers, respectively). Consequently, the scaling of the variables and parameters results in the approximate correspondence of one-time unit in the models to 1.44 times the half-life of the second monomer B. After generating the dimensionless kinetic models (see Supplementary Information), we utilized them to investigate Hopf bifurcations and eventually identified Turing patterns within the models with the added diffusive terms.

PDE model construction

For each model, we introduced diffusive terms into the ordinary differential equations, transforming them into partial differential equations. To standardize the diffusive terms, we scaled the equations using a spatial scaling parameter (r_0). The spatial scaling parameter r_0 (i.e. one unit length) in our models has values spanning the range of 1.6–3207 μm . Typically, one spatial unit in our models represents 363 μm which roughly corresponds to 24 times the median diameter of human epithelial cells. The PDEs for all models are included in Supplementary Information. For example, the PDE system of the AB-1 network is given as:

$$\begin{aligned} \partial[A]/\partial t &= 1 - \chi_A[A] + \kappa^{\text{off}}[AB] - \kappa^{\text{on}}[A][B] + \beta_{AB}[AB] + D_A \nabla^2[A] \\ \partial[B]/\partial t &= \sigma_B - [B] - \kappa^{\text{on}}[A][B] + \kappa^{\text{off}}[AB] + \chi_A \alpha_{AB}[AB] + D_B \nabla^2[B] \\ \partial[AB]/\partial t &= \kappa^{\text{on}}[A][B] - \kappa^{\text{off}}[AB] - \alpha_{AB}[AB] - \beta_{AB}[AB] + D_{AB} \nabla^2[AB], \end{aligned} \quad (1)$$

where [A], [B] and [AB] represent the dimensionless concentrations of free A, free B, and AB complex, respectively. The parameters in Eq. 1 were also dimensionless. σ_B represents the transcription rate constant of B. κ^{on} represents the association rate constant. κ^{off} represents the dissociation rate constant. χ_A is the degradation rate constant of A. α_{AB} and β_{AB} are regulated degradation factors (RDFs). α_{AB} represents how fast A is degraded in the complex relative to its unbound form, and β_{AB} is the corresponding factor for B. D_A , D_B and D_{AB} are diffusion coefficients for the three molecular species. ∇^2 is the Laplacian operator. The meanings of other parameters in other models are defined similarly.

Together with other four models, we analytically proved that Eq. 1 cannot have any unstable steady state with arbitrary positive rate constants, even though Eq. 1 has implicit feedback loops whose structures were considered sufficient to generate Turing patterns (see Supplementary Information).

Algebraic analysis

We adopted a search by negation approach to analyze the Turing pattern in these biochemical reaction networks. As the initial step, we employed analytical approaches to eliminate models that could not induce instability in the system. The linear stability analysis of models containing one or two components dismisses their capacity to exhibit any form of pattern-enabling bifurcation. For models comprising more than two components, we conducted the analysis with the Routh-Hurwitz Criterion^{27,28}, which led to the elimination of three additional models. However, models with more than three components did not provide conclusive results during the analysis with the Routh-Hurwitz Criterion. Therefore, following the algebraic analysis, 18 models are left for further investigation. Previous studies on systematic search for pattern-enabling networks typically combined analytical and computational approaches for screening reaction diffusion systems. We used a similar strategy in this work (as described in

the following three sections). Nonetheless, we expect that more sophisticated algebraic methods will be useful for analyzing the 18 networks more efficiently.

ODE parameter sampling and numerical bifurcation analysis

To explore the intriguing dynamical characteristics of the remaining 18 models, we employed numerical continuation techniques to conduct bifurcation analysis. To cover the entire biologically plausible parameter space, we randomly sampled 10^4 parameter sets for each model. We used log-uniform distributions of the parameters using established ranges of biologically feasible values covering two orders of magnitude, as detailed in the Supplementary Information (Supplementary Table S1).

The synthesis rate constant of species B (σ_B) (or σ_A for single-subunit systems) served as the control parameter for numerical bifurcation analysis, quantifying the steady-state signal-response relationship within the range of 0 to 120. The initial equilibrium point was obtained with numerical simulation at $\sigma_B = 0$ (or $\sigma_A = 0$ for single subunit systems) using randomized initial conditions, and each of the 18 systems has a single positive equilibrium point under this condition (see Supplementary Information). The Tellurium package (version 2.2.4) in python⁶⁴, which includes a plugin of an implementation of AUTO⁶⁵, was used to detect local bifurcation (e.g. Hopf bifurcation and saddle-node bifurcation) points (Supplementary Fig. S4). The bifurcation analysis reveals that there are 10 different networks leading to 6 different complexes that show Hopf bifurcation and are capable of Turing pattern formation.

PDE parameter sampling and dispersion analysis

Eventually, to pinpoint the specific parameter space conducive to Turing pattern formation, we sampled 4000 diffusive parameter sets for each of the ODE parameter sets that resulted in Hopf bifurcation during numerical bifurcation analysis. We sampled the diffusion coefficients so that the median value of the distribution aligns with the diffusion coefficients of the macromolecules inside the cell. For each of the diffusive parameter sets we formulated a Jacobian matrix of the dynamical system and evaluated the maximum real part of the eigenvalues for a series of wavenumbers (with a step size of $\Delta q = 0.05$, equivalent to a detection resolution of approximately $4.75 \times 10^3 \mu\text{m}$) using the NumPy module in python. The graph depicting maximum real eigenvalue against the wave number produces the dispersion curve for the system at that specific parameter set. We can anticipate the emergence of Turing patterns only if there is a positive real eigenvalue at a finite wave number.

Numerical Simulation

To corroborate our dispersion analysis results (particularly to confirm that pattern formation was not disrupted by far-away stable equilibria⁶⁶), we chose parameter sets with potentially less stiffness for each of the 10 pathways capable of pattern formation. Subsequently, we simulated the partial differential equations using the explicit Euler method. Detailed information about the simulation is provided in the Supplementary Information.

Estimation of instances of pattern-enabling complexes based on omics data

We used databases of human protein complex and protein-protein interactions to relate our model predicted complex configurations that enabled Turing patterns to experimentally identified protein associations. At the proteomic level, we used hu.MAP 2.0 to enumerate over 7000 complexes based on integrated data from large scale affinity purification mass spectrometry⁴⁰. Instances of model predicted configurations were estimated based on whether each complex configuration (e.g. AAB) matches a subset of protein subunits in each complex in the dataset. Because large complexes can give rise to too

many smaller complexes combinatorially, we estimated the number of protein subunits that are involved in each configuration via the formation of any experimentally identified complex. We also confirmed pair-wise protein associations, which provided evidence supporting intermediate complexes leading to the final complex formation, using STRING database with the physical interaction constraint on the protein-protein links⁶⁷. We performed functional enrichment of protein subunits involved in high-order complexes that potentially permit pattern formation (Fig. 6a. Boxes). We used a background set of 7471 proteins in the human secretome and membrane proteome, presumably subject to long-range transport⁵¹. We performed the enrichment analysis for 747 proteins that were both involved in potentially pattern-enabling complexes and in the secretome with this background.

We estimated the instances of mRNA-microRNA complexes using TargetScan, a microRNA target prediction package⁴¹. To avoid combinatorial prediction of small RNA complexes from mRNAs with many microRNA binding sites, we estimated the number of human mRNAs that are involved in configurations predicted by the models. For example, AAB can represent an mRNA carrying two conserved binding sites for the same microRNA. The functional enrichment of the mRNAs in potentially pattern-enabling complexes was performed with standard background.

Statistics & reproducibility

No statistical method was used to predetermine sample size. Sample size was chosen to give sufficient resolution of parameter regions for pattern formation. No data were excluded from the analyses. The analyses and simulations were performed through computer programs in an unbiased manner. Investigators were therefore blinded to allocation and outcome assessment.

Reporting summary

Further information on research design is available in the Nature Portfolio Reporting Summary linked to this article.

Data availability

All relevant data supporting the key findings of this study are available within the article and its Supplementary Information files. The simulation data generated in this study are provided in the Source Data files. Source data are provided with this paper.

Code availability

All code required to reproduce results in this study, including algebraic analyses, computational work and PDE simulations, be found at https://github.com/shibashispaul32/Turing_Reaction_Networks⁶⁸. The repository also provides links for performing example simulations interactively without coding via VisualPDE web interface⁶⁹.

References

1. Turing, A. M. The chemical basis of morphogenesis. *Philos. Trans. R. Soc. Lond. B. Biol. Sci.* **237**, 37–72 (1952).
2. Gandhi, P., Ciocanel, M.-V., Niklas, K. & Dawes, A. T. Identification of approximate symmetries in biological development. *Philos. Trans. R. Soc. A* **379**, 20200273 (2021).
3. Jung, H.-S. et al. Local inhibitory action of BMPs and their relationships with activators in feather formation: implications for periodic patterning. *Dev. Biol.* **196**, 11–23 (1998).
4. Nakamasu, A., Takahashi, G., Kanbe, A. & Kondo, S. Interactions between zebrafish pigment cells responsible for the generation of Turing patterns. *Proc. Natl. Acad. Sci. USA* **106**, 8429–8434 (2009).
5. Glover, J. D. et al. The developmental basis of fingerprint pattern formation and variation. *Cell* **186**, 940–956 (2023).
6. Glover, J. D. et al. Hierarchical patterning modes orchestrate hair follicle morphogenesis. *PLoS Biol.* **15**, e2002117 (2017).

7. Raspopovic, J., Marcon, L., Russo, L. & Sharpe, J. Digit patterning is controlled by a Bmp-Sox9-Wnt Turing network modulated by morphogen gradients. *Science* **345**, 566–570 (2014).
8. Aragón, J. L., Torres, M., Gil, D., Barrio, R. A. & Maini, P. K. Turing patterns with pentagonal symmetry. *Phys. Rev. E* **65**, 051913 (2002).
9. Veerman, F., Mercker, M. & Marciniak-Czochra, A. Beyond Turing: far-from-equilibrium patterns and mechano-chemical feedback. *Philos. Trans. R. Soc. A* **379**, 20200278 (2021).
10. Wolpert, L. Positional information and the spatial pattern of cellular differentiation. *J. Theor. Biol.* **25**, 1–47 (1969).
11. Cooke, J. & Zeeman, E. C. A clock and wavefront model for control of the number of repeated structures during animal morphogenesis. *J. Theor. Biol.* **58**, 455–476 (1976).
12. Green, J. & Sharpe, J. Positional information and reaction-diffusion: two big ideas in developmental biology combine. *Development* **142**, 1203–1211 (2015).
13. Tewary, M. et al. A stepwise model of reaction-diffusion and positional information governs self-organized human peri-gastrulation-like patterning. *Development* **144**, 4298–4312 (2017).
14. Hannezo, E. & Heisenberg, C.-P. Mechanochemical feedback loops in development and disease. *Cell* **178**, 12–25 (2019).
15. Pantoja-Hernández, J., Breña-Medina, V. F. & Santillán, M. Hybrid reaction-diffusion and clock-and-wavefront model for the arrest of oscillations in the somitogenesis segmentation clock. *Chaos: Interdiscip. J. Nonlinear Sci.* **31**, 063107 (2021).
16. Cheng, X. & Ferrell, J. E. Jr Spontaneous emergence of cell-like organization in *Xenopus* egg extracts. *Science* **366**, 631–637 (2019).
17. Gierer, A. & Meinhardt, H. A theory of biological pattern formation. *Kybernetik* **12**, 30–39 (1972).
18. Landge, A. N., Jordan, B. M., Diego, X. & Müller, P. Pattern formation mechanisms of self-organizing reaction-diffusion systems. *Dev. Biol.* **460**, 2–11 (2020).
19. Murray, J. D. *Mathematical biology II: Spatial models and biomedical applications*. Vol. 3 (Springer New York, 2001).
20. Kondo, S. & Miura, T. Reaction-diffusion model as a framework for understanding biological pattern formation. *Science* **329**, 1616–1620 (2010).
21. Scholes, N. S., Schnoerr, D., Isalan, M. & Stumpf, M. P. H. A comprehensive network atlas reveals that Turing patterns are common but not robust. *Cell Syst.* **9**, 243–257 (2019).
22. Marcon, L., Diego, X., Sharpe, J. & Müller, P. High-throughput mathematical analysis identifies Turing networks for patterning with equally diffusing signals. *eLife* **5**, e14022 (2016).
23. Diego, X., Marcon, L., Müller, P. & Sharpe, J. Key features of Turing systems are determined purely by network topology. *Phys. Rev. X* **8**, 021071 (2018).
24. Waters, F. R., Yates, C. A. & Dawes, J. H. P. Minimal reaction schemes for pattern formation. *J. R. Soc. Interface* **21**, 20230490 (2024).
25. Epstein, I. R. & Pojman, J. A. in *An Introduction to Nonlinear Chemical Dynamics: Oscillations, Waves, Patterns, and Chaos* (eds Epstein, I. R. & Pojman, J. A.) **0** (Oxford University Press, 1998).
26. Woolley, T. E., Krause, A. L. & Gaffney, E. A. Bespoke Turing systems. *Bull. Math. Biol.* **83**, 1–32 (2021).
27. Routh, E. J. *A Treatise on the Stability of a Given State of Motion, Particularly Steady Motion: Being the Essay to which the Adams Prize was Adjudged in 1877, in the University of Cambridge*. (Macmillan and Company, 1877).
28. Hurwitz, A. Ueber die Bedingungen, unter welchen eine Gleichung nur Wurzeln mit negativen reellen Theilen besitzt. *Mathematische Ann.* **46**, 273–284 (1895).
29. Cross, M. C. & Hohenberg, P. C. Pattern formation outside of equilibrium. *Rev. Mod. Phys.* **65**, 851–1112 (1993).
30. Jensen, O., Pannbacker, V. O., Dewel, G. & Borckmans, P. Subcritical transitions to Turing structures. *Phys. Lett. A* **179**, 91–96 (1993).
31. Lengyel, I. & Epstein, I. R. A chemical approach to designing Turing patterns in reaction-diffusion systems. *Proc. Natl. Acad. Sci. USA* **89**, 3977–3979 (1992).
32. Krause, A. L., Gaffney, E. A., Maini, P. K. & Klika, V. Modern perspectives on near-equilibrium analysis of Turing systems. *Philos. Trans. R. Soc. A* **379**, 20200268 (2021).
33. Cross, M. & Greenside, H. *Pattern formation and dynamics in nonequilibrium systems*. (Cambridge University Press, 2009).
34. Rovinsky, A. B. & Menzinger, M. Self-organization induced by the differential flow of activator and inhibitor. *Phys. Rev. Lett.* **70**, 778 (1993).
35. Rubinstein, B. Y., Mattingly, H. H., Berezhkovskii, A. M. & Shvartsman, S. Y. Long-term dynamics of multisite phosphorylation. *Mol. Biol. Cell* **27**, 2331–2340 (2016).
36. Obatake, N., Shiu, A., Tang, X. & Torres, A. Oscillations and bistability in a model of ERK regulation. *J. Math. Biol.* **79**, 1515–1549 (2019).
37. Nordick, B., Yu, P. Y., Liao, G. & Hong, T. Nonmodular oscillator and switch based on RNA decay drive regeneration of multimodal gene expression. *Nucleic Acids Res* **50**, 3693 (2022).
38. Klika, V., Baker, R. E., Headon, D. & Gaffney, E. A. The influence of receptor-mediated interactions on reaction-diffusion mechanisms of cellular self-organisation. *Bull. Math. Biol.* **74**, 935–957 (2012).
39. Rovinsky, A. B. & Menzinger, M. Chemical instability induced by a differential flow. *Phys. Rev. Lett.* **69**, 1193 (1992).
40. Drew, K., Wallingford, J. B. & Marcotte, E. M. hu. MAP 2.0: integration of over 15,000 proteomic experiments builds a global compendium of human multiprotein assemblies. *Mol. Syst. Biol.* **17**, e10016 (2021).
41. Agarwal, V., Bell, G. W., Nam, J.-W. & Bartel, D. P. Predicting effective microRNA target sites in mammalian mRNAs. *eLife* **4**, e05005 (2015).
42. Li, B. et al. Impaired Wnt/ β -catenin pathway leads to dysfunction of intestinal regeneration during necrotizing enterocolitis. *Cell Death Dis.* **10**, 743 (2019).
43. Geetha-Loganathan, P., Nimmagadda, S. & Scaal, M. Wnt signaling in limb organogenesis. *Organogenesis* **4**, 109–115 (2008).
44. Zhu, X. et al. Wls-mediated Wnts differentially regulate distal limb patterning and tissue morphogenesis. *Dev. Biol.* **365**, 328–338 (2012).
45. Montanari, M. P., Tran, N. V. & Shimmi, O. Regulation of spatial distribution of BMP ligands for pattern formation. *Dev. Dyn.* **251**, 178–192 (2022).
46. Shu, W., Jiang, Y. Q., Lu, M. M. & Morrissey, E. E. Wnt7b regulates mesenchymal proliferation and vascular development in the lung. *Development* **129**, 4831–4842 (2002).
47. Copeland, J., Wilson, K. & Simoes-Costa, M. Micromanaging pattern formation: miRNA regulation of signaling systems in vertebrate development. *FEBS J.* **289**, 5166–5175 (2022).
48. Ferretti, E. et al. Concerted microRNA control of Hedgehog signalling in cerebellar neuronal progenitor and tumour cells. *EMBO J.* **27**, 2616–2627 (2008).
49. Li, C. J. MicroRNA governs bistable cell differentiation and lineage segregation via a noncanonical feedback. *Mol. Syst. Biol.* **17**, e9945 (2021).
50. Hu, Q. et al. Clinical applications of exosome membrane proteins. *Precis. Clin. Med.* **3**, 54–66 (2020).
51. Uhlén, M. et al. Tissue-based map of the human proteome. *Science* **347**, 1260419 (2015).
52. Zheng, M. M., Shao, B. & Ouyang, Q. Identifying network topologies that can generate Turing pattern. *J. Theor. Biol.* **408**, 88–96 (2016).
53. Grimson, A. et al. MicroRNA targeting specificity in mammals: determinants beyond seed pairing. *Mol. Cell* **27**, 91–105 (2007).
54. Eichhorn, S. W. et al. mRNA destabilization is the dominant effect of mammalian microRNAs by the time substantial repression ensues. *Mol. Cell* **56**, 104–115 (2014).

55. Hemming, M. L., Elias, J. E., Gygi, S. P. & Selkoe, D. J. Proteomic profiling of γ -secretase substrates and mapping of substrate requirements. *PLoS Biol.* **6**, e257 (2008).
56. Harrell, M. A. et al. Arp2/3-dependent endocytosis ensures Cdc42 oscillations by removing Pak1-mediated negative feedback. *J. Cell Biol.* **223**, e202311139 (2024).
57. Economou, A. D., Monk, N. A. M. & Green, J. B. A. Perturbation analysis of a multi-morphogen Turing reaction-diffusion stripe patterning system reveals key regulatory interactions. *Development* **147**, dev190553 (2020).
58. Gaffney, E. A. & Monk, N. A. M. Gene expression time delays and Turing pattern formation systems. *Bull. Math. Biol.* **68**, 99–130 (2006).
59. Korvasová, K., Gaffney, E. A., Maini, P. K., Ferreira, M. A. & Klika, V. Investigating the Turing conditions for diffusion-driven instability in the presence of a binding immobile substrate. *J. Theor. Biol.* **367**, 286–295 (2015).
60. Sargood, A., Gaffney, E. A. & Krause, A. L. Fixed and distributed gene expression time delays in reaction–diffusion systems. *Bull. Math. Biol.* **84**, 98 (2022).
61. Xu, C., Tyson, J. J. & Cao, Y. Turing-pattern model of scaffolding proteins that establish spatial asymmetry during the cell cycle of *Caulobacter crescentus*. *Iscience* **26**, 106513 (2023).
62. Ding, B., Itaya, A. & Qi, Y. Symplasmic protein and RNA traffic: regulatory points and regulatory factors. *Curr. Opin. Plant Biol.* **6**, 596–602 (2003).
63. O'Brien, K., Breyne, K., Ughetto, S., Laurent, L. C. & Breakefield, X. O. RNA delivery by extracellular vesicles in mammalian cells and its applications. *Nat. Rev. Mol. Cell Biol.* **21**, 585–606 (2020).
64. Choi, K. et al. Tellurium: an extensible python-based modeling environment for systems and synthetic biology. *Biosystems* **171**, 74–79 (2018).
65. Doedel, E. J. AUTO: A program for the automatic bifurcation analysis of autonomous systems. *Congr. Numer* **30**, 265–284 (1981).
66. Krause, A. L., Gaffney, E. A., Jewell, T. J., Klika, V. & Walker, B. J. Turing instabilities are not enough to ensure pattern formation. *Bull. Math. Biol.* **86**, 21 (2024).
67. Szklarczyk, D. et al. The STRING database in 2023: protein–protein association networks and functional enrichment analyses for any sequenced genome of interest. *Nucleic Acids Res.* **51**, D638–D646 (2023).
68. Paul, S., Hong, T. Widespread biochemical reaction networks enable Turing patterns without imposed feedback. Computer code for 'Widespread biochemical reaction networks enable Turing patterns without imposed feedback' v. 1. <https://doi.org/10.5281/zenodo.13368447> (2024).
69. Walker, B. J., Townsend, A. K., Chudasama, A. K. & Krause, A. L. VisualPDE: rapid interactive simulations of partial differential equations. *Bull. Math. Biol.* **85**, 113 (2023).

Acknowledgements

This work is supported by grants from National Institutes of Health (R35GM149531) and from National Science Foundation (2243562) awarded to T.H.

Author contributions

Conceptualization: S.P. and T.H. Formal analysis: S.P and T.H. Simulation: S.P and T.H. Data analysis: S.P and T.H. Bioinformatics analysis: S.P, J.A., and T.H. Visualization: S.P. and T.H. Supervision: T.H. Funding acquisition: T.H.

Competing interests

The authors declare no competing interests.

Additional information

Supplementary information The online version contains supplementary material available at <https://doi.org/10.1038/s41467-024-52591-0>.

Correspondence and requests for materials should be addressed to Tian Hong.

Peer review information *Nature Communications* thanks Jing Chen and Andrew Krause for their contribution to the peer review of this work. A peer review file is available.

Reprints and permissions information is available at <http://www.nature.com/reprints>

Publisher's note Springer Nature remains neutral with regard to jurisdictional claims in published maps and institutional affiliations.

Open Access This article is licensed under a Creative Commons Attribution-NonCommercial-NoDerivatives 4.0 International License, which permits any non-commercial use, sharing, distribution and reproduction in any medium or format, as long as you give appropriate credit to the original author(s) and the source, provide a link to the Creative Commons licence, and indicate if you modified the licensed material. You do not have permission under this licence to share adapted material derived from this article or parts of it. The images or other third party material in this article are included in the article's Creative Commons licence, unless indicated otherwise in a credit line to the material. If material is not included in the article's Creative Commons licence and your intended use is not permitted by statutory regulation or exceeds the permitted use, you will need to obtain permission directly from the copyright holder. To view a copy of this licence, visit <http://creativecommons.org/licenses/by-nc-nd/4.0/>.

© The Author(s) 2024